

Quantum probe hyperpolarisation of molecular nuclear spins

David A. Broadway,^{1,2,*} Jean-Philippe Tetienne,^{1,2} Alastair Stacey,^{1,3} James D. A. Wood,^{1,2,4} David A. Simpson,² Liam T. Hall,^{2,†} and Lloyd C. L. Hollenberg^{1,2,‡}

¹*Centre for Quantum Computation and Communication Technology,
School of Physics, University of Melbourne, Parkville, VIC 3010, Australia*

²*School of Physics, University of Melbourne, Parkville, VIC 3010, Australia*

³*Melbourne Centre for Nanofabrication, Clayton, VIC 3168, Australia*

⁴*Department of Physics, University of Basel, Klingelbergstrasse 82, 4056, Basel, Switzerland*

The hyperpolarisation of nuclear spins within target molecules is a critical and complex challenge in magnetic resonance imaging (MRI) [1] and nuclear magnetic resonance (NMR) spectroscopy [2]. Hyperpolarisation offers enormous gains in signal and spatial resolution which may ultimately lead to the development of molecular MRI and NMR [3]. At present, techniques used to polarise nuclear spins generally require low temperatures and/or high magnetic fields, radiofrequency control fields, or the introduction of catalysts or free-radical mediators [4–7]. The emergence of room temperature solid-state spin qubits has opened exciting new pathways to circumvent these requirements to achieve direct nuclear spin hyperpolarisation using quantum control [6, 8]. Employing a novel cross-relaxation induced polarisation (CRIP) protocol, we demonstrate the first external nuclear spin hyperpolarisation achieved by a quantum probe, in this case of ¹H molecular spins in poly(methyl methacrylate). In doing so, we show that a single qubit is capable of increasing the thermal polarisation of $\sim 10^6$ nuclear spins by six orders of magnitude, equivalent to an applied magnetic field of 10^5 T. The technique can also be tuned to multiple spin species, which we demonstrate using both ¹³C and ¹H nuclear spin ensembles. Our results are analysed and interpreted via a detailed theoretical treatment, which is also used to describe how the system can be scaled up to a universal quantum hyperpolarisation platform for the production of macroscopic quantities of contrast agents at high polarisation levels for clinical applications. These results represent a new paradigm for nuclear spin hyperpolarisation for molecular imaging and spectroscopy, and beyond into areas such as materials science and quantum information processing.

With the prospect of molecular MRI [3] revolutionising many areas of research and clinical applications, the generation of hyperpolarised molecular targets attracts intense interest. Well known techniques include high-field/low temperature brute-force methods [4], dynamic nuclear polarisation [6], optical pumping [5], and parahydrogen induced polarisation [7]. On the other hand, the rapid advances in semiconductor spin qubit technology for quantum computing [9, 10] and quantum sensing [11, 12] has opened up the exciting possibility of hyperpolarising nuclear spins at a fundamental level via quantum mechanical protocols [6, 8, 13–20]. Despite early progress [21, 22], the application of quantum probe technology to this problem still faces a number of significant challenges. To be of practical use, a quantum probe must be capable of polarising a relatively large number of remote nuclear spins external to the probe substrate, ideally under ambient conditions. We address these challenges using a quantum spin probe in diamond as an entropy pump, and demonstrate polarisation of external molecular spin ensembles over relatively large volumes at room temperature, with the prospect of scaling up to a universal hyperpolarisation platform suitable for clinical applications. In contrast to existing methods, our quantum polarisation approach is tunable to a range of nuclear species, operates at room temperature, and is inherently free of radiofrequency (RF) fields and extraneous chemistry.

For this study, we employ a nitrogen-vacancy (NV)

quantum spin probe in a diamond substrate (Fig. 1a) [11]. The protocol employs an external magnetic field, B , to tune the ground-state spin transition frequency of the NV (ω_{NV}) into resonance with target nuclear spins (ω_{n}) (Fig. 1b). For a given target species, the spin resonance condition is fulfilled at a magnetic field $B_*(\gamma_{\text{n}}) \approx 2D/(\gamma_{\text{NV}} - \gamma_{\text{n}})$ [23], where γ_{n} , γ_{NV} are the target and NV gyromagnetic ratios, and D is the NV zero-field splitting (Fig. 1c). Entropy pumping is facilitated by repeated application of the cross relaxation induced polarisation (CRIP) sequence (Fig. 1d), wherein the NV spin is optically initialised into $|0\rangle$ state and the NV-target hyperfine interaction is allowed to occur for a given period of time, τ (of order microseconds). The transfer of magnetisation caused by this interaction thus polarises the target spins into their $|\downarrow\rangle$ state (Fig. 1c). For the sake of comparison, depolarisation may be facilitated by interleaving the initialisation of the NV spin into the opposite state $|-1\rangle$ by the application of an RF π -pulse (Fig. 1e).

To quantitatively understand the effect of the CRIP protocol on the target spin ensemble, we developed a microscopic theory that explicitly includes the dipole interactions of ensemble spins and their interaction with a single NV quantum probe (see Supplementary Information for details). We define the polarisation of a spin at position \mathbf{R} (relative to the NV) and time t to be $P(\mathbf{R}, t)$;

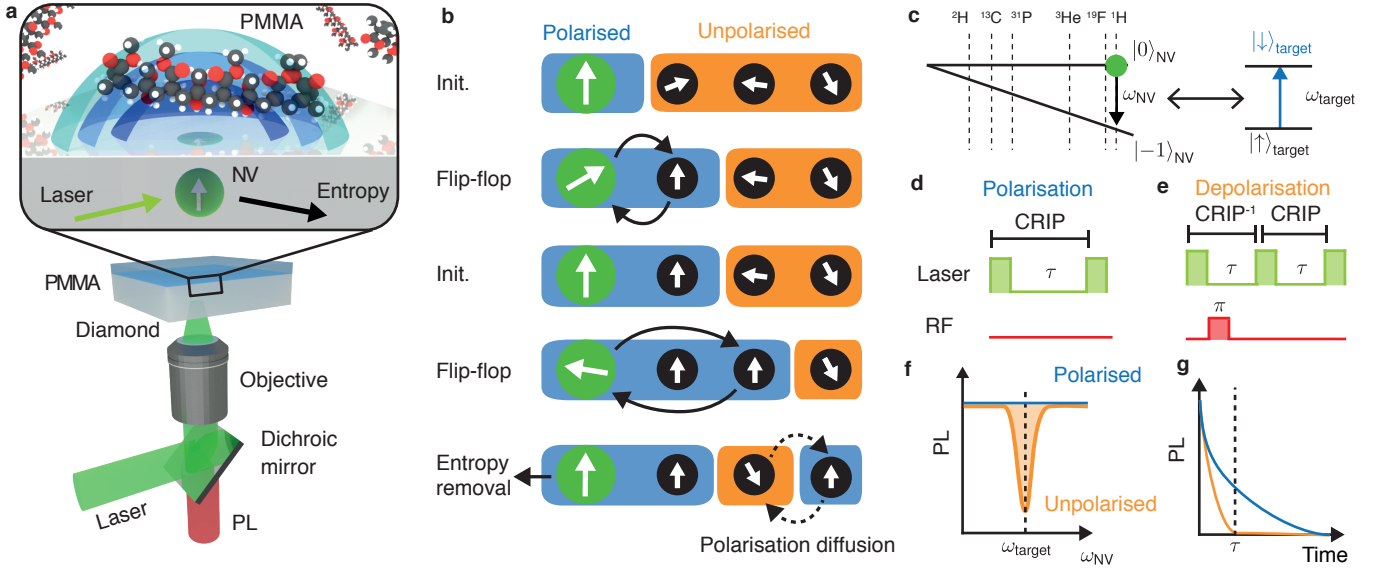


FIG. 1. **Quantum probe hyperpolarisation of nuclear spin ensembles.** **a**, Schematic of the system showing a near-surface nitrogen-vacancy (NV) spin probe in diamond and a hydrogen nuclear spin target ensemble in molecular Poly(methyl methacrylate) (PMMA) on the surface. The NV probe is initialised by a green laser (532 nm), and read out via its photoluminescence (PL) signal. The shaded blue surfaces denote different regimes of polarisation capabilities arising from the spatial dependence of the nuclear spin coupling to the NV qubit. **b**, Schematic of cross relaxation induced polarisation (CRIP) implemented on a spin system illustrating the build up of polarisation from repeated application of the CRIP sequence. Diffusion effects act in competition with the CRIP entropy pumping mechanism, but also allow for polarisation at distances beyond that reachable via the hyperfine interaction. **c**, Energy-level diagram of the NV showing the relative positions of various target nuclear spin resonance conditions. **d,e**, The control sequences laser pulses in green, RF pulses in red) used for polarising a target spin ensemble using CRIP (**d**) and for controlled depolarisation using the combined $\text{CRIP}^{-1} \times \text{CRIP}$ protocol (**e**). **f**, Schematic showing the cross-relaxation spectrum obtained by measuring the PL during the CRIP (blue) or depolarisation (orange) sequence with a constant interaction time τ , while scanning the NV frequency ω_{NV} . **g**, Similarly, the cross-relaxation curve is obtained by scanning τ with ω_{NV} set at the resonance.

with the evolution of $P(\mathbf{R}, t)$ described by

$$\frac{\partial}{\partial t} P(\mathbf{R}, t) = (\beta \nabla^2 - u(\mathbf{R}) - \Gamma_{\text{SL}}) P(\mathbf{R}, t) + u(\mathbf{R}), \quad (1)$$

subject to an initial unpolarised state $P(\mathbf{R}, t) = 0$; where $u(\mathbf{R}) = A^2(\mathbf{R})/2\Gamma_2$ is the effective cooling coefficient resulting from the hyperfine coupling $A(\mathbf{R})$ with the NV spin, Γ_2 is the dephasing rate of the NV spin β is the effective polarisation diffusion coefficient related to the intra-target interactions, and Γ_{SL} is the spin-lattice relaxation rate of the target spin ensemble. This formulation allows us to predict and describe the spatial extent of polarisation for a given target sample of arbitrary geometry.

To probe the polarisation effect experimentally, we monitor the spin-dependent photoluminescence (PL) from the NV [24–26] during the laser pulses, which decays as a function of the CRIP sequence time as $e^{-\Gamma_{\text{tot}}\tau}$. Here Γ_{tot} is the NV longitudinal relaxation rate, which can be expressed as the sum $\Gamma_{\text{tot}} = \Gamma_{\text{bg}} + \Gamma_{\text{CR}}$, where Γ_{bg} is the background rate caused by lattice phonons or surface effects, and Γ_{CR} is due to cross-relaxation. The latter follows a Lorentzian dependence on the detuning

between the probe and target transition frequencies[24],

$$\Gamma_{\text{CR}} = \frac{A_P^2 \Gamma_2}{2\Gamma_2^2 + 2(\omega_{\text{NV}} - \omega_n)^2}, \quad (2)$$

where A_P^2 is the total hyperfine field variance seen by the NV due to the target ensemble, which is related to the polarisation distribution via

$$A_P^2 = \frac{n_t}{2} \int [1 - P(\mathbf{R}, t)] A^2(\mathbf{R}) d^3\mathbf{R}, \quad (3)$$

where n_t is the density of the target spin ensemble. The key indicator of significant polarisation is therefore a reduction in Γ_{CR} , which manifests as the disappearance of the target ensemble’s spectral feature from the cross-relaxation spectrum (Fig. 1f), and can be quantified by measuring the cross-relaxation curve at resonance (Fig. 1g).

Experimentally, we first demonstrate our technique on the inherent 1.1% ^{13}C spin ensemble surrounding a NV probe in the diamond substrate by tuning to the ^{13}C resonant condition at $B_*(^{13}\text{C}) = 1024.9$ G. Comparison of the cross-relaxation spectra for CRIP and depolarisation sequences (Fig. 2a) shows the complete removal of

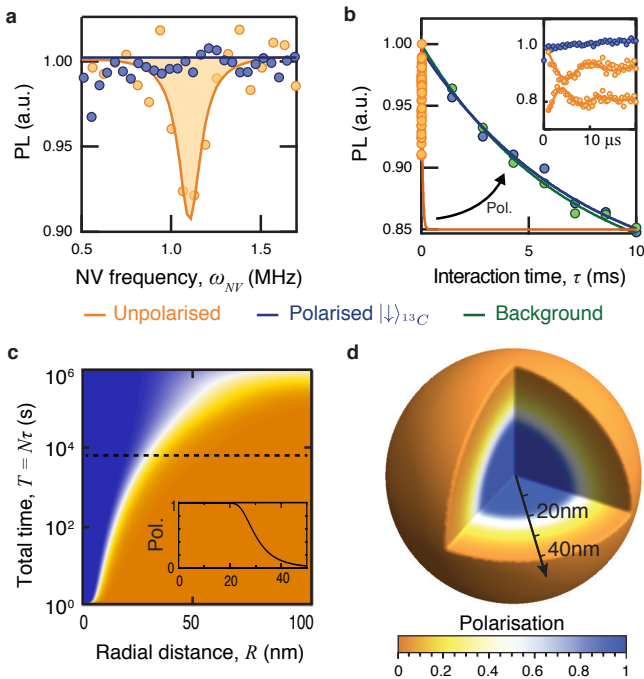


FIG. 2. **Cross-relaxation induced polarisation of ^{13}C spins in diamond.** **a**, Cross-relaxation spectra of a single NV spin near the ^{13}C resonance ($\omega_{\text{NV}} = 1.1$ MHz), obtained with an interaction time $\tau = 4$ μs using the CRIP sequence (blue) and the depolarisation sequence (orange, only the readout following the NV initialisation in $|0\rangle$ is shown). Sequences were repeated $N = 10^5$ times at each point. **b**, Cross-relaxation curves obtained by increasing τ at the ^{13}C resonance with the CRIP sequence (blue) and depolarisation sequence (orange), and off-resonance to obtain the background relaxation curve (green). Zoom-in at short times for the polarised (blue) and unpolarised case (orange, top and bottom curves correspond to the NV initialised in $|0\rangle$ and $|-1\rangle$, respectively). **c**, Calculated radial polarisation profiles relative to the NV spin (averaged over all angles), calculated from Eq. (1) for a random 1.1% ^{13}C spin ensemble for varying total polarisation times, $T = N\tau$. Inset: profile along dashed line, corresponding to $T = 2$ h. **d**, Three-dimensional representation of the polarisation distribution at $T = 2$ h.

the ^{13}C resonance peak for interaction times of $\tau = 4$ μs , indicating efficient polarisation of the nearest spins, as compared with the target prepared using the depolarising sequence. This is confirmed in the cross-relaxation curves as a function τ (Fig. 2b, inset), where the polarised case shows no evolution of the NV spin state, while the unpolarised case shows coherent flip-flops between the NV and the ^{13}C spins.

To investigate the extent of the polarisation effect, we increase the interaction time τ so as to be sensitive to more remote ^{13}C spins, up to the limit set by the NV centre's intrinsic spin-phonon relaxation rate, $\Gamma_{\text{bg}} \approx 200$ ms^{-1} . The resulting cross-relaxation curves obtained at the ^{13}C resonance using the CRIP and depolarisation sequences are shown in Fig. 2b, from which

we extract the total relaxation rate, Γ_{tot} . By subtracting Γ_{bg} obtained from the off-resonance relaxation curve (Fig. 2b, green data), we deduce the ^{13}C -induced relaxation rate $\Gamma_{\text{CR}} = \Gamma_{\text{tot}} - \Gamma_{\text{bg}}$, which decreases from $\Gamma_{\text{CR}}^{\text{unpol}} \approx 250$ ms^{-1} with the depolarisation sequence, to below the noise floor of the measurement after 5 hours of CRIP, $\Gamma_{\text{CR}}^{\text{pol}} \approx 19$ s^{-1} . We use Eq. (1) (with $\beta = 0.0335$ nm^2s^{-1} corresponding to the given ^{13}C density) to calculate the time-dependence of the radial polarisation profile for total polarisation times of 1-10⁶ s, as depicted in Fig 2c. By relating the spatial polarisation distribution, $P(\mathbf{R}, t)$, to the cross-relaxation rate, Γ_{CR} , via Eq. (2), we find the theoretical results are consistent with the experiment for polarisation times in excess of two hours (Fig. 2c, dashed line). Examination of the spatial polarisation distribution (Fig. 2c, inset, and Fig. 2d) implies a polarisation level of more than 99% within 21 nm of the NV, equating to a 6×10^6 -fold increase on thermal polarisation for 3×10^5 spins.

With the basic protocol established, we now move to the polarisation of molecular ^1H nuclear spins external to the diamond crystal. A solution of poly(methyl methacrylate), PMMA, was applied directly to a diamond substrate [12] with single NV spin probes located 8-12 nm below the surface. CRIP was applied with the external magnetic field tuned to resonance at $B_*(^1\text{H}) = 1026.2$ G. With a much higher diffusion constant and spin-lattice relaxation rate ($\beta = 781$ nm^2s^{-1} , $\Gamma_{\text{SL}} = 1$ s^{-1}) relative to the intrinsic ^{13}C case, the ^1H system effectively reaches steady-state within a few seconds. Application of the CRIP sequence to NV1 (data for other NVs are shown in the Supplementary Information) for $\tau = 20$ μs (Fig. 3a) shows the removal of the hydrogen spectral feature (blue), as compared with the depolarising sequence (orange). From the cross-relaxation curves after 1 hour of CRIP (Fig 3b), we extract ^1H -induced rates for the unpolarised ($\Gamma_{\text{CR}}^{\text{unpol}}$) and polarised ($\Gamma_{\text{CR}}^{\text{pol}}$) PMMA ^1H spin ensembles to be 2.71 ms^{-1} and 0.96 ms^{-1} , respectively. The ratio $\Gamma_{\text{CR}}^{\text{unpol}}/\Gamma_{\text{CR}}^{\text{pol}} = 2.8(3)$ (consistent with the value of 2.4(3) obtained using another NV), is in good agreement with the solution to Eq. (1) for the PMMA ensemble, which gives a ratio of 2.2 in the steady state. The corresponding spatial polarisation distribution is shown in Fig. 3c, indicating that the system reaches 50% average polarisation over a volume of $\sim (26$ nm)³. Thus, we conclude that the single spin quantum probe has increased the average polarisation of roughly a million hydrogen spins by some six orders of magnitude over the room temperature Boltzmann thermal background.

There is scope for improvement on these proof-of-concept results: for example, engineering NV depths to 5 nm would increase the rate of target spin polarisation by an order of magnitude, and improvements in the inherent NV dephasing rate Γ_2 (e.g. via im-

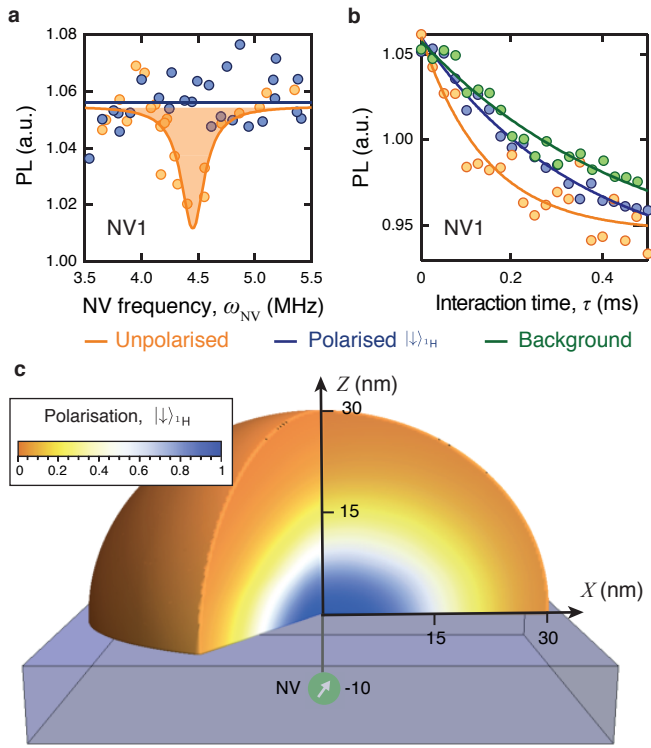


FIG. 3. **Polarisation of external molecular ^1H spins.** **a**, Cross-relaxation spectra near the ^1H resonance ($\omega_{\text{NV}} = 4.4$ MHz), for a single NV spin located 10 nm below a PMMA layer, obtained using $\tau = 20 \mu\text{s}$ and $N = 10^5$ with the CRIP sequence (blue) and the depolarisation sequence (orange). **b**, Cross-relaxation curves obtained by increasing τ at the ^1H resonance with the CRIP sequence (blue) and depolarisation sequence (orange), and off-resonance to obtain the background relaxation rate (green). **c**, Three-dimensional representation of the ^1H spin polarisation distribution in the PMMA, calculated from Eq. (1) in the steady state.

proved surface properties) will allow for more precise tuning to different nuclear spin species. As the protocol is all optical, scaling up for high-volume production could be achieved by stacking multiple NV arrays (Fig. 4a) and/or increasing the effective interaction area via surface patterning [27]. The results presented here indicate that the CRIP protocol could produce macroscopic quantities of MRI contrast agents with high polarisation levels. For example, we consider ^{13}C isotopically enriched HEP (hydroxyethyl propionate, $^{13}\text{C}_5\text{H}_{10}\text{O}_3$), a well-known MRI contrast agent [28]. Using a single hyperpolarisation cell comprised of two NV arrays in diamond membranes separated by $1 \mu\text{m}$ (see zoomed schematic in Fig. 4a; we assume an NV density of $4 \times 10^{11} \text{cm}^{-2}$ over a $4 \text{mm} \times 4 \text{mm}$ diamond surface [29]), the rate of polarisation transfer to a concentrated 1M precursor HEP solution is $4 \mu\text{L/s}$ at a polarisation level of 80%. The polarisation levels for different contrast agents in 1M precursor solutions are plotted against polarisation time

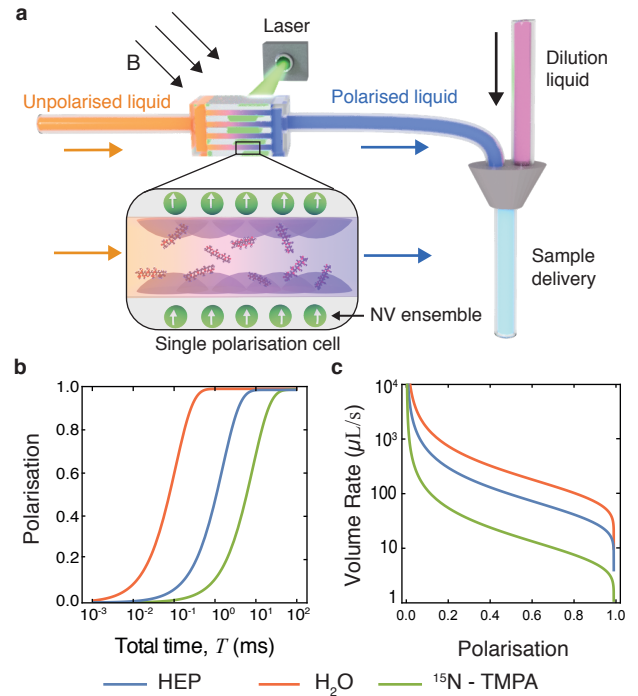


FIG. 4. **Scale-up for a universal MRI contrast agent hyperpolarisation platform.** **a**, Schematic of a quantum polarisation stack comprising multiple diamond membranes, each containing NV array layers on both sides, in a homogeneous magnetic field tuned to the nuclear gyromagnetic ratio of the target agent spin species. The unpolarised agent in concentrated solution (orange) flows into the stack channels, where the liquid is polarised through the application of CRIP (via a pulsed laser). The out-flowing polarised liquid (blue) is then diluted for use. Zoomed schematic shows a single polarisation cell comprising a channel formed by dual diamond membranes each with a near-surface NV layer. **b**, Average polarisation level from a single polarisation cell, for various targets (HEP, H_2O , and ^{15}N -TMPA), calculated for varying polarisation times assuming perfect mixing of a 1 M target agent solution with a cell height of $1 \mu\text{m}$. **c**, Outflow rate (after dilution to 1mM for application delivery) from 10 polarisation cells at different levels of polarisation.

(assuming perfect mixing occurs over these timescales) in Fig. 4b. In Fig. 4c, we plot the final delivery rate after dilution to 1 mM for a stack of 10 cells, showing that delivery rates of order $100 \mu\text{L/s}$ for clinical applications [30] are achievable.

In summary, we have experimentally demonstrated hyperpolarisation of molecular nuclear spins under ambient conditions by employing a quantum spin probe entropy pump. The technique works at low field, room temperature, requires no RF fields, and operates directly on the target molecules without the need for catalysts or free radicals. With high polarisation rates and tunability, there are excellent prospects for scale-up of the system to produce macroscopic quantities of a range of contrast agents at polarisation levels required for molecular

MRI/NMR. The technique can be extended to other nuclear spin species and may also offer new pathways in quantum information for initialisation of quantum simulators, or increasing the fidelity of operations through spin-bath neutralisation.

Author Contributions: The CRIP protocol was conceived by LTH. Experiments were performed by DAB and J-PT, with input from AS, DAS, JDAW, LTH, and LCLH. LTH developed the theory, with input from LCLH. DAB, J-PT, AS, and DAS prepared the samples. LCLH, DAB and LTH wrote the manuscript with input from all authors. LCLH supervised the project.

Acknowledgements: This work was supported in part by the Australian Research Council (ARC) under the Centre of Excellence scheme (project No. CE110001027). This work was performed in part at the Melbourne Centre for Nanofabrication (MCN) in the Victorian Node of the Australian National Fabrication Facility (ANFF). L.C.L.H. acknowledges the support of an ARC Laureate Fellowship (project No. FL130100119). J.-P.T acknowledges support from the ARC through the Discovery Early Career Researcher Award scheme (DE170100129) and the University of Melbourne through an Establishment Grant and an Early Career Researcher Grant. D.A.B is supported by an Australian Government Research Training Program Scholarship.

Competing Interests: The authors declare that they have no competing financial interests.

Correspondence: Correspondence and requests for materials should be addressed to L.C.L.H. (email: lloydch@unimelb.edu.au), D.A.B (email: broadway@student.unimelb.edu.au), or L.T.H (email: liam.hall@unimelb.edu.au).

* broadway@student.unimelb.edu.au

† liam.hall@unimelb.edu.au

‡ lloydch@unimelb.edu.au

- [1] Christopher deCharms, R. Applications of real-time fMRI. *Nature Reviews Neuroscience* **9**, 720–729 (2008).
- [2] Rossini, A. J. *et al.* Dynamic Nuclear Polarization Surface Enhanced NMR Spectroscopy. *Accounts of Chemical Research* **46**, 1942–1951 (2013).
- [3] Nikolaou, P., Goodson, B. M. & Chekmenev, E. Y. NMR Hyperpolarization Techniques for Biomedicine. *Chemistry - A European Journal* **21**, 3156–3166 (2015).
- [4] Bajaj, V. *et al.* Dynamic nuclear polarization at 9T using a novel 250GHz gyrotron microwave source. *Journal of Magnetic Resonance* **160**, 85–90 (2003).
- [5] Viteau, M. *et al.* Optical Pumping and Vibrational Cooling of Molecules. *Science* **321** (2008).
- [6] London, P. *et al.* Detecting and Polarizing Nuclear Spins with Double Resonance on a Single Electron Spin. *Physical Review Letters* **111**, 067601 (2013).
- [7] Bhattacharya, P. *et al.* Parahydrogen-induced polarization (PHIP) hyperpolarized MR receptor imaging in vivo: a pilot study of ^{13}C imaging of atheroma in mice. *NMR in Biomedicine* **24**, 1023–1028 (2011).
- [8] Álvarez, G. A. *et al.* Local and bulk ^{13}C hyperpolarization in nitrogen-vacancy-centred diamonds at variable fields and orientations. *Nature Communications* **6**, 8456 (2015).
- [9] Morello, A. *et al.* Single-shot readout of an electron spin in silicon. *Nature* **467**, 687–691 (2010).
- [10] Zwanenburg, F. A. *et al.* Silicon quantum electronics. *Reviews of Modern Physics* **85**, 961–1019 (2013).
- [11] Doherty, M. W. *et al.* The nitrogen-vacancy colour centre in diamond. *Physics Reports* **528**, 1–45 (2013).
- [12] Mamin, H. J. *et al.* Nanoscale Nuclear Magnetic Resonance with a Nitrogen-Vacancy Spin Sensor. *Science* **339**, 557–560 (2013).
- [13] Knowles, H. S., Kara, D. M. & Atatüre, M. Demonstration of a Coherent Electronic Spin Cluster in Diamond. *Physical Review Letters* **117**, 100802 (2016).
- [14] Belthangady, C. *et al.* Dressed-State Resonant Coupling between Bright and Dark Spins in Diamond. *Physical Review Letters* **110**, 157601 (2013).
- [15] Wang, H.-J. *et al.* Sensitive magnetic control of ensemble nuclear spin hyperpolarization in diamond. *Nature Communications* **4** (2013).
- [16] Fischer, R. *et al.* Bulk Nuclear Polarization Enhanced at Room Temperature by Optical Pumping. *Physical Review Letters* **111**, 057601 (2013).
- [17] King, J. P. *et al.* Room-temperature in situ nuclear spin hyperpolarization from optically pumped nitrogen vacancy centres in diamond. *Nature Communications* **6**, 8965 (2015).
- [18] Chen, Q., Schwarz, I., Jelezko, F., Retzker, A. & Plenio, M. B. Optical hyperpolarization of C 13 nuclear spins in nanodiamond ensembles. *Physical Review B - Condensed Matter and Materials Physics* **92** (2015). 1504.02368.
- [19] Liu, G.-Q. *et al.* Protection of centre spin coherence by dynamic nuclear spin polarization in diamond. *Nanoscale* **6**, 10134–9 (2014).
- [20] Rej, E., Gaebel, T., Boele, T., Waddington, D. E. J. & Reilly, D. J. Hyperpolarized nanodiamond with long spin-relaxation times. *Nature Communications* **6**, 8459 (2015).
- [21] Abrams, D., Trusheim, M. E., Englund, D., Shattuck, M. D. & Meriles, C. A. Dynamic Nuclear Spin Polarization of Liquids and Gases in Contact with Nanostructured Diamond Dynamic Nuclear Spin Polarization of Liquids and Gases in Contact with Nanostructured Diamond. *Nano letters* **5** (2014).
- [22] Chen, Q., Schwarz, I., Jelezko, F., Retzker, A. & Plenio, M. B. Resonance-inclined optical nuclear spin polarization of liquids in diamond structures. *Physical Review B - Condensed Matter and Materials Physics* **93**, 060408 (2016).
- [23] Broadway, D. A. *et al.* Anticrossing Spin Dynamics of Diamond Nitrogen-Vacancy Centers and All-Optical Low-Frequency Magnetometry. *Physical Review Applied* **6**, 064001 (2016).
- [24] Hall, L. T. *et al.* Detection of nanoscale electron spin resonance spectra demonstrated using nitrogen-vacancy centre probes in diamond. *Nature Communications* **7**, 10211 (2016).
- [25] Wood, J. D. A. *et al.* Microwave-Free Nuclear Magnetic Resonance at Molecular Scales (2016). 1610.01737.

- [26] Wood, J. D. A. *et al.* Wide-band, nanoscale magnetic resonance spectroscopy using quantum relaxation of a single spin in diamond. *Physical Review B - Condensed Matter and Materials Physics* **94**, 1–16 (2016).
- [27] Kehayias, P. *et al.* Solution nuclear magnetic resonance spectroscopy on a nanostructured diamond chip (2017). 1701.01401.
- [28] Schmidt, A. B. *et al.* Liquid-state carbon-13 hyperpolarization generated in an MRI system for fast imaging. *Nature Communications* **8**, 14535 (2017).
- [29] Simpson, D. A. *et al.* Quantum magnetic resonance microscopy (2017). 1702.04418.
- [30] Golman, K., in 't Zandt, R. & Thaning, M. Real-time metabolic imaging. *Proceedings of the National Academy of Sciences of the United States of America* **103**, 11270–5 (2006).